Gating the Selectivity Filter in ClC Chloride Channels

Raimund Dutzler, *et al.*

Science **300**, 108 (2003);
DOI: 10.1126/science.1082708

C isotopic composition is solar and the anomalous Xe and N have low abundances.
38. B.-G. Choi, G. J. Wasserburg, G. R. Huss, *Astrophys. J.* **522**, L133 (1999).
39. L.R. Nittler *et al.*, *Lunar Planet. Sci.* **34**, Abstract 1703 (2003).
40. G. Huss, A. J. Fahey, R. Gallino, G. J. Wasserburg, *Astrophys. J.* **430**, L81 (1994)
41. I. D. Hutcheon, G. R. Huss, A. J. Fahey, G. J. Wasserburg, *Astrophys. J.* **425**, L97 (1994).
42. N. Krestina, W. Hsu, G. J. Wasserburg, *Lunar Planet. Sci.* **33**, A1425 (2002).
43. L. R. Nittler, C. M. O'D. Alexander, J. Wang, X. Gao, *Nature* **393**, 222 (1998).
44. E. Zinner *et al.*, in preparation.
45. Supported by NASA grants NAG5-9801 and RTOP 344-31-40-07. This work was enabled by the revolutionary NanoSIMS ion microprobe, which was designed by G. Slodzian at the University of Orsay, Paris.

18 November 2002; accepted 19 February 2003
Published online 27 February 2003;
10.1126/science.1080576
Include this information when citing this paper.

Gating the Selectivity Filter in ClC Chloride Channels

Raimund Dutzler, Ernest B. Campbell, Roderick MacKinnon*

ClC channels conduct chloride (Cl^-) ions across cell membranes and thereby govern the electrical activity of muscle cells and certain neurons, the transport of fluid and electrolytes across epithelia, and the acidification of intracellular vesicles. The structural basis of ClC channel gating was studied. Crystal structures of wild-type and mutant *Escherichia coli* ClC channels bound to a monoclonal Fab fragment reveal three Cl^- binding sites within the 15-angstrom neck of an hourglass-shaped pore. The Cl^- binding site nearest the extracellular solution can be occupied either by a Cl^- ion or by a glutamate carboxyl group. Mutations of this glutamate residue in *Torpedo* ray ClC channels alter gating in electrophysiological assays. These findings reveal a form of gating in which the glutamate carboxyl group closes the pore by mimicking a Cl^- ion.

Ion channels carry electric current across the membrane of cells in the form of diffusing ions. The two key properties of ion channels are selective ion conduction and gating. Selective conduction refers to a channel's ability to select one ionic species among those present in the cellular environment and catalyze its rapid flow through the pore; gating refers to opening and closing the pore, the process by which ion conduction is turned on or off.

In some channels, the functions of selective conduction and gating are mediated by quite separate structural elements. Potassium channels, for example, have a selectivity filter near the extracellular side of the pore and a gate near the intracellular side (*1*). Separation of the filter and gate allows ligand-binding domains or voltage sensor domains to open and close the pore through large conformational changes without affecting the selectivity filter, whose structure must be maintained in order to discriminate among ions on the basis of their small differences in radius (*2–4*).

Years of electrophysiological study suggest that the condition of a structurally independent selectivity filter and gate will probably not apply to ClC channels, a large Cl^- channel family whose members are found from bacteria to animals (*5–7*). In ClC channels, selective conduction and a certain form of gating referred to as "fast gating" seem to be intimately coupled to each other. Chloride ions conduct rapidly through the pore, and at the same time they affect the probability that the fast gate will be open (*8, 9*). Certain ClC channels have even been called "Cl^--activated Cl^- channels" because extracellular Cl^- causes the gate to open (*8, 9*). Membrane voltage can influence the open probability as well, but even this property depends on Cl^- ions (*8, 9*).

We sought to understand the structural origins of gating in ClC channels and why gating is closely tied to Cl^- ion conduction. Specifically, we tested a possibility raised by the first ClC channel structures: that a glutamate side-chain carboxyl group gates the pore by binding to a Cl^- ion site within the selectivity filter (*10*).

Structure of a ClC channel bound to a Fab. A reasonably high-resolution structure was required in order to define the Cl^- ion coordination chemistry within the conduction pore with accuracy. To this end, monoclonal antibodies were raised and a crystal structure of an *E. coli* ClC channel bound to a Fab fragment was determined at 2.5 Å resolution (*11*) (Table 1). A single Fab was attached to the extracellular

Howard Hughes Medical Institute, Laboratory of Molecular Neurobiology and Biophysics, Rockefeller University, 1230 York Avenue, New York, NY 10021, USA.

*To whom correspondence should be addressed. E-mail: mackinn@rockvax.rockefeller.edu

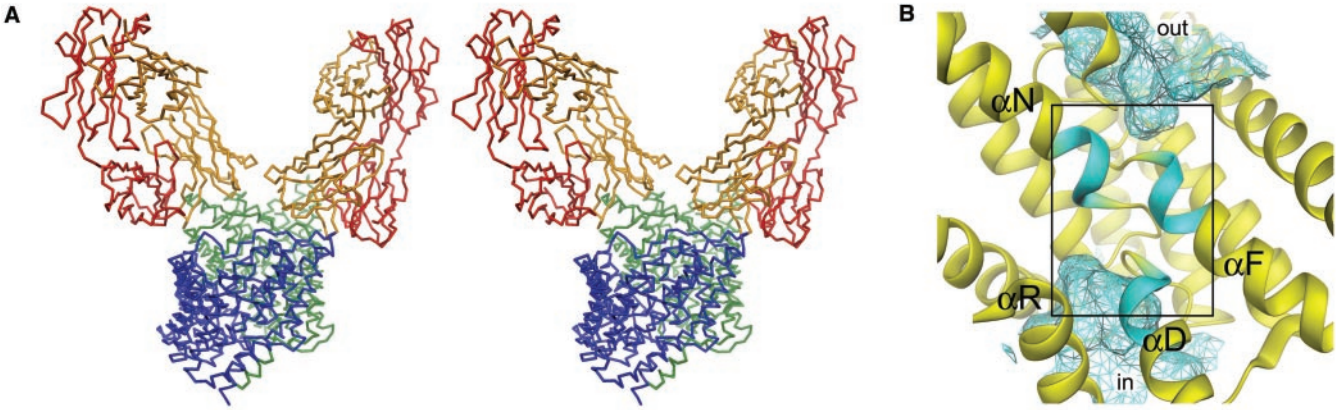

Fig. 1. Structure of the EcClC Fab complex. (**A**) Stereo view of a Cα representation of the EcClC channel in complex with two Fab fragments. The complex is viewed at an angle of about 30° from the plane of the membrane. The two ClC subunits are colored blue and green; the light and heavy chains of the two Fab fragments are colored red and orange, respectively. (**B**) View of the ion-conducting pore of the ClC subunit. The pore is viewed from the dimer interface, with foreground α helices removed for clarity. The protein is shown as a ribbon. The N-terminal ends of α helices D, F, and N are cyan. Aqueous cavities from the extracellular solution (out) and intracellular solution (in) are shown as cyan mesh. The selectivity filter is indicated by a black frame. Figures 1, 2, and 4 were prepared with DINO (www.dino3d.org).

surface of each subunit in the homodimeric channel (Fig. 1A). As demonstrated previously, each identical subunit within the dimer forms its own independent pore for Cl^- ions; that is, a ClC dimer is really two Cl^- channels stuck together (*10*) (PDB accession codes 1KPK and 1KPL). The pore within each subunit is shaped roughly like an hourglass with a selectivity filter forming a narrow neck partway across the membrane, connecting wide water-filled vestibules from the intracellular and extracellular solutions (Fig. 1B). The channel has an antiparallel architecture, meaning that it is made of two structurally similar domains that are related by a pseudo two-fold symmetry axis lying within the plane of the membrane. This architecture places the selectivity filter at the pseudo two-fold axis with the "positive" N termini of helices αN and αF positioned to stabilize Cl^- ions inside the membrane (Fig. 1B).

The present study focuses exclusively on the region outlined by the rectangle in Fig. 1B. Figure 2 shows the atomic details of this region. The $(F_{Br} - F_{Cl})$ isomorphous difference electron density map (red mesh) superimposed on the averaged native protein electron density map (blue mesh) reveals two halogen ions bound in the selectivity filter (Fig. 2A). One of these, labeled S_{cen} for central site, was described in the original crystal structure (*10*). This ion is coordinated by main-chain amide nitrogen atoms from the end of helix αN and from the side chains of conserved amino acids Ser^{107} and Tyr^{445} (Fig. 2B). The second ion, labeled S_{int} for internal site, is located at the interface where the aqueous vestibule from the intracellular solution meets the selectivity filter. This ion is coordinated on one side by main-chain amide nitrogen atoms from the end of helix αD, and on the other side it is exposed to the vestibule (Fig. 2B). At the opposite end of the selectivity filter, near the opening into the extracellular vestibule, the side chain of Glu^{148} is obstructing the pore with its carboxyl group inserted between the ends of helices αN and αF, bridging the helices together through hydrogen bonding. This location of a glutamate side chain in the ion conduction pathway led us to propose that our crystal structure is of a closed channel, and that the glutamate serves as a gate. We used a combination of electrophysiology and x-ray crystallography to test this possibility.

Function of ClC-0 channels with an altered glutamate gate. Because we are unable to study bacterial ClC channels using electrophysiological methods, we studied channel function with ClC-0 from the *Torpedo* ray expressed in *Xenopus* oocytes (*12*) (Fig. 3) (*13, 14*). Comparing the function of ClC-0 with the structure of the *E. coli* ClC channel is not optimal but is well justified by the high degree of conservation within the selectivity filter of ClC channels, including the glutamate residue in question.

ClC-0 channels in oocytes exhibit fast gating, which is voltage-dependent and therefore can be studied by changing the membrane voltage (Fig. 3A) (*13*). The fast gate closes at negative (inside relative to outside) membrane voltages and opens upon depolarization to positive voltages. In Fig. 3A, closure of the fast gate is manifest by the gradual reduction of inward (downward) current over time after steps to negative test voltages. The fraction of open channels at different membrane voltages is estimated by measuring the current immediately after returning to a fixed control voltage. The slope of the curve relating open probability to membrane voltage corresponds to a valence of around 1.0, as if a single electron charge crosses the membrane voltage difference in association with movement of the fast gate (Fig. 3B) (*8, 9*).

When Glu^{166} is mutated to Ala, Gln, or Val, the qualitative effect on channel function is the same; the fast gate appears to stay open (Fig. 3, C to E). This effect is most obvious at very negative test voltages where the gradual reduction of inward current observed in the wild-type channel is nearly absent, as if the mutations abolish or diminish fast gating. At the level of single-channel analysis, mutation of the glutamate residue causes both pores to remain open most of the time (Fig. 3G). The double-barrel nature of the channel is still evident because of rare excursions from level 2 (two pores open) to level 1 (one pore open) and even rarer visits to level 0 (both pores closed). The channel record hints that the single-pore closure rate (corresponding to fast gate closure) is slower in the mutant than in the wild type and that the single-pore opening rate is faster. Whether these residual closures represent side chain occlusion or, more likely, a separate "occlusion" process is unknown. But it is clear that the fast gating process is markedly altered when the glutamate is mutated.

We note also a more subtle "mutation"—that caused by lowering the pH of the extracellular solution (Fig. 3F). This maneuver causes the wild-type channel to behave much like mutant ClC-0 channels in which the glutamate residue has been replaced by another amino acid. Chen and co-workers carried out a detailed analysis of pH effects on fast gating (*15*) and showed that extracellular pH influences the rate of channel opening but not closing. In the context of the ClC channel structure, we interpret the effect of pH on gating to mean that the deprotonated (anionic) form of the glutamate side chain closes the wild-type channel. One might ask why the channel is open at pH 5.0

Table 1. Summary of data collection and refinement statistics. All crystals are of space group C_2 (a = 230 Å, b = 94 Å, c = 169 Å, α = δ = 90°, β = 131.5°), with one ClC dimer and two Fab fragments in the asymmetric unit. Data for the wild-type *E. coli* ClC (wt EcClC) FAB Cl^- complex were collected at CHESS A1; all other data sets were collected at NSLS X25. Indexing, integration, and scaling were carried out with DENZO and SCALEPACK (*24*). The structure of the wt EcClC Fab complex was solved by molecular replacement with AMORE (*25*) using the StCLC structure (PDB code 1KPK) as well as a Fab structure (PDB code 1K4C) as search models. Initial phases were calculated from the rigid-body refined Fab substructure alone. The phases were improved by solvent flattening and two-fold domain averaging, breaking the complex structure into three domains (channel, Fv region, and Fc region) with DM (*26*). The model was built with the program O (*27*) and refined with CNS (*28*) by iterative cycles of simulated annealing and model rebuilding. R_{free} was monitored throughout the refinement. The final model contains 13,224 protein atoms, four Cl^- ions, and 443 water molecules. The same set of reflections was set aside for the calculation of R_{free} in the wild-type and mutant structures. The structure solution of the E148A and E148Q mutants was initiated by rigid-body refinement of the wt EcClC Fab complex with the respective data set. The structures were refined in alternating cycles of simulated annealing and model rebuilding. RMSD, root mean square difference; numbers in parentheses correspond to the highest resolution shell.

Data collection

	Wavelength (Å)	Resolution (Å)	Completeness (%)	R_{merge}* (%)	$I/\sigma I$
wt EcClC FAB complex					
Cl^-	0.93	35 to 2.5	96.6 (94.1)	4.8 (56.9)	20.5 (2.3)
Br^-	1.1	35 to 2.8	90.0 (54.7)	4.8 (19.0)	14.7 (3.9)
EcClC E148A FAB complex					
Cl^-	1.1	35 to 3.0	93.7 (76.2)	7.2 (49.2)	14.8 (2.1)
Br^-	0.916	35 to 4.0	94.7 (94.5)	7.6 (33.2)	15.2 (3.7)
EcClC E148Q FAB complex					
Cl^-	1.1	35 to 3.3	96.9 (93.2)	7.5 (42.9)	13.6 (2.1)
Br^-	1.1	35 to 4.1	93.5 (80.3)	9.5 (48.1)	14.4 (2.8)

Refinement

	Resolution (Å)	R_{free}/R_{cryst}†	RMSD (bond/angles)
wt EcClC FAB	25 to 2.5	29.9/26.4	0.01/1.3
EcClC E148A FAB	25 to 3.0	33.8/29.6	0.01/1.4
EcClC E148Q FAB	25 to 3.3	32.5/29.4	0.01/1.5

*$R_{merge} = \Sigma\Sigma|I - I_j|/\Sigma I$. †$R_{cryst} = \Sigma|F_p - F_{p(calc)}|/\Sigma|F_p|$.

when the expected pK_a for glutamate is closer to 4.0. We propose that the pK_a of the glutamate is perturbed toward a physiological pH because it is very near (~4 Å) to a Cl^- ion. In summary, it appears that whether the glutamate residue is altered by mutation or by protonation, the ability to close the pore by a fast gating process is diminished. These observations support the idea that the glutamate residue gates the pore of ClC channels.

Structures of the pore with an altered glutamate gate. We determined crystal structures of two mutant *E. coli* ClC channels: Glu^{148} → Ala (E148A) and Glu^{148} → Gln (E148Q) (Fig. 4). In the E148A mutant channel, a halogen anion is observed in place of the glutamate side chain, shown by the strong peak labeled S_{ext} for external site in the ($F_{Br}^+ - F_{Br}^-$) anomalous difference Fourier map (red mesh) calculated from crystals grown in Br^- solution. When Glu^{148} is mutated, we think that the pore is open because it contains an uninterrupted queue of anions connecting the intracellular and extracellular solutions (Fig. 4, A and B). The S_{ext} site is located exactly between the N termini of helices αF and αN, where amide nitrogen atoms form a cage surrounding the ion. An ion at this site comes in contact exclusively with main-chain amide nitrogen atoms; this chemistry suggests that the S_{ext} site is important for selective ion conduction through the open channel. It is notable that the S_{ext} and S_{cen} sites are only 4 Å apart. Although we do not have rigorous crystallographic evidence that these sites are occupied simultaneously, the closed structure with an anionic glutamate and a Cl^- ion in the pore would argue that they are.

The structure of the E148Q mutant channel shows what the wild-type channel might look like while in its conducting conformation (Fig. 4, C and D). An ($F_{Br} - F_{Cl}$) isomorphous difference electron density map (red mesh) shows that ions bind at all three sites in this channel, as in the E148A mutant. But the glutamine side chain is directed toward the extracellular solution, rather than into the pore. It seems reasonable to think that the glutamate side chain may assume a somewhat similar conformation in the open, conducting conformation of the wild-type channel.

Discussion. The structural and functional data presented here are consistent with the picture of gating outlined in Fig. 5. The proposed mechanism is very simple: When the S_{ext} site is occupied by the glutamate carboxyl group, the pore is closed or blocked; when the site is occupied by a Cl^- ion, the pore is open or conductive. Figure 5 pertains specifically to what is referred to as the "fast gate" in ClC-0, which governs each pore independently and is distinct from a "slow gate" that opens and closes both pores simultaneously (*16*). The glutamate gate very nicely explains two important characteristic properties of the fast gating process: that the two pores are gated independently (*13*) and that the fast gate within each pore is coupled to Cl^- ions (*8, 9*).

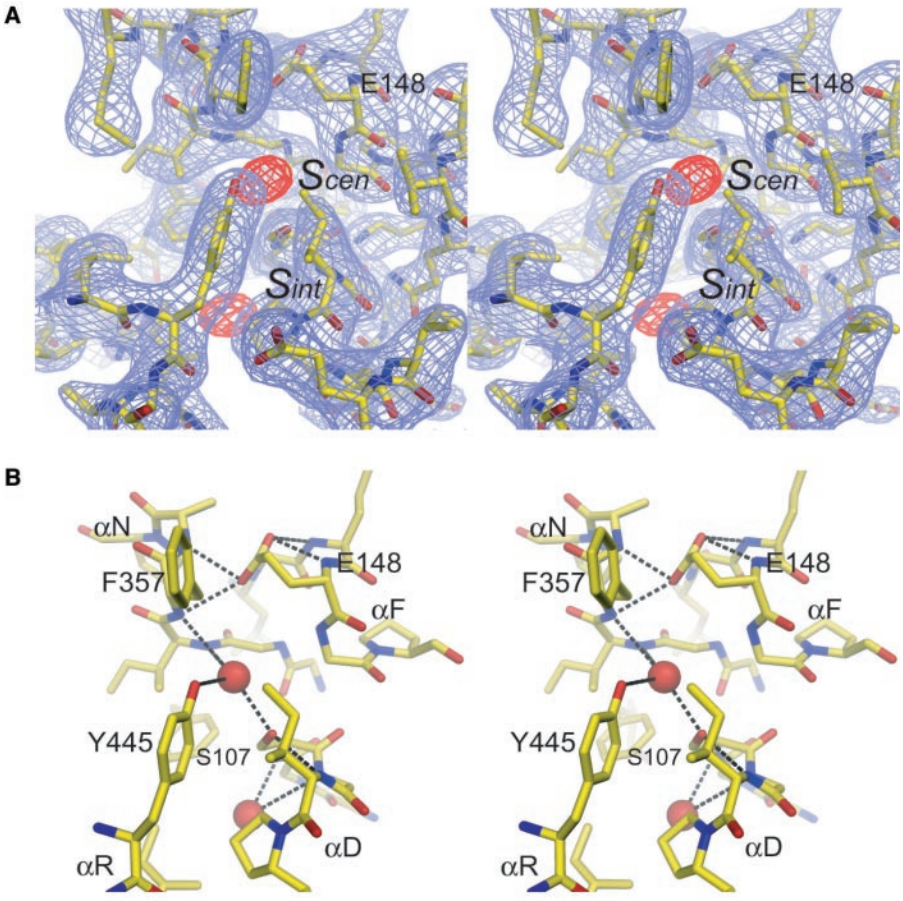

Fig. 2. Structure of the selectivity filter of the wild-type EcClC Fab complex. (**A**) Stereo view of electron density in the selectivity filter at 2.5 Å, contoured at 1σ. The view is from the dimer interface within the membrane. The cytoplasm is on the bottom, the extracellular side on the top. The map was calculated from native amplitudes and solvent-flattened two-fold averaged phases. The refined protein model is shown as sticks. An ($F_{Br} - F_{Cl}$) difference Fourier map at 2.8 Å, contoured at 4σ, is shown in red. (**B**) Stereo view of the ion-binding sites. Selected residues in the vicinity of the bound chloride ions are shown. Hydrogen bonds between the protein and chloride ions (red spheres) as well as between the side chain of Glu^{148} and the rest of the protein are shown as black dashed lines.

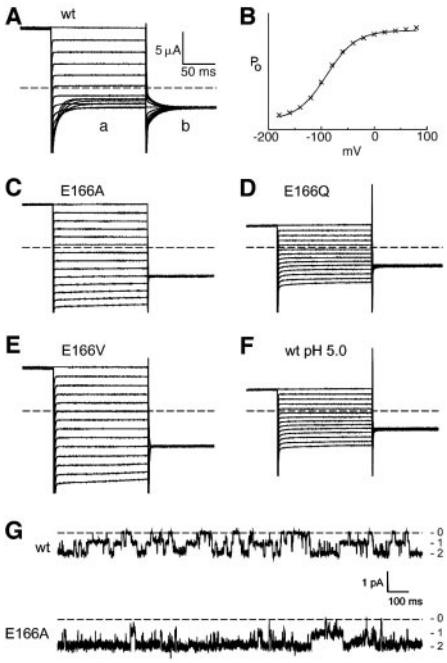

Fig. 3. Voltage-dependent gating in ClC-0. (**A**) Whole-cell oocyte currents of the wild-type (wt) channel. Current traces were recorded using a previously described protocol (*8*). Voltage pulses ranging from +80 to –180 mV (a) precede a step to a test pulse at –100 mV (b). (**B**) Voltage-dependent gating of the wt channel was analyzed by plotting the current 7 ms after stepping to the test pulse at –100 mV against the preceding voltage. Data points were fitted to a Boltzmann function, $P_o(V) = 1/\{1 + \exp[-z_n e_0(V - V_{1/2})/kT]\}$, where e_0 is the elementary charge, $V_{1/2}$ is the voltage of half-maximal activation, k is the Boltzmann constant, T is absolute temperature, and $z_n = 0.92$ is the valence. (**C** to **F**) Whole-cell currents of the mutants E166A, E166Q, and E166V and wt at pH 5.0 are recorded using the same voltage protocol as in (A). (**G**) Single-channel traces of wt (top) and E166A mutant (bottom) EcClC channels recorded at –80 mV with 5 mM Hepes (pH 7.5), 110 mM *N*-methyl-D-glucamine (NMDG)–Cl, 5 mM $MgCl_2$, and 1 mM $CaCl_2$ inside, and 5 mM Hepes (pH 7.5), 110 mM NaCl, 5 mM $MgCl_2$, and 1 mM EGTA outside.

The independent gating of two pores was described more than 20 years ago by Miller (*13*). He used this property to deduce that ClC channels must contain two identical pores by essentially noting that ClC channels in single-channel records always seemed to appear as two independently gated channels. The glutamate gate is entirely consistent with independent gates because each pore contains its own glutamate residue, and most important, the conformational change associated with gating within an individual pore is small and local, limited to the swing of an amino acid side chain. The small conformational change associated with gating in one pore is unlikely to influence gating in the other, thus allowing their independence.

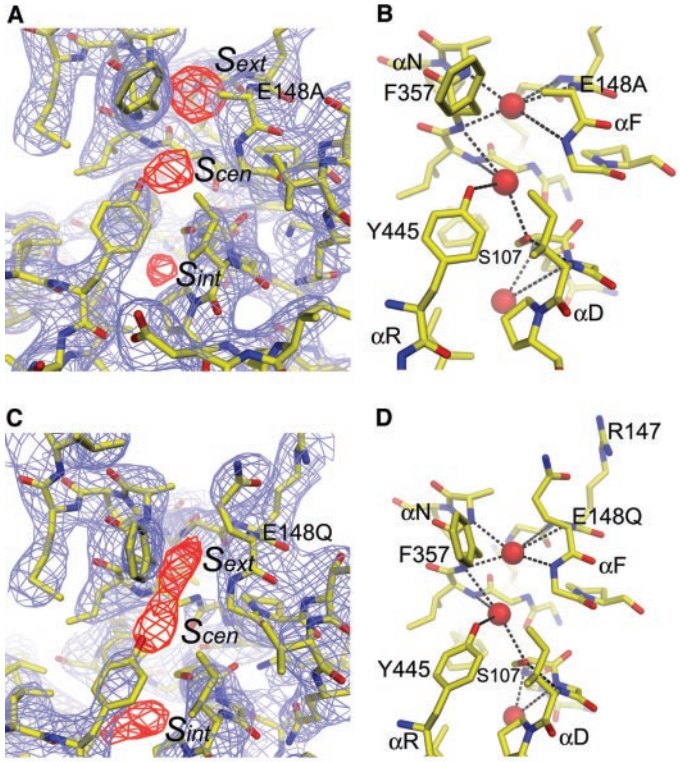

Fig. 4. Structure of the selectivity filter of mutant EcClC Fab complexes. (**A**) Electron density in the selectivity filter of the EcClC E148A mutant at 3.0 Å. The view is the same as in Fig. 2. The map was calculated from native amplitudes and solvent-flattened two-fold averaged phases and is contoured at 1σ. The refined protein model is shown as sticks. An anomalous difference Fourier map at 4.0 Å from crystals grown in Br^-, contoured at 5.5σ, is shown in red. (**B**) View of the ion-binding sites of the EcClC E148A mutant. Selected residues in the vicinity of the bound chloride ions are shown. Hydrogen bonds between the protein and chloride ions (red spheres) are shown as dashed lines. (**C**) Electron density in the selectivity filter of the EcClC E148Q mutant at 3.3 Å. The map was calculated from native amplitudes and solvent-flattened two-fold averaged phases and is contoured at 1σ. An ($F_{Br} - F_{Cl}$) difference Fourier map at 4.1 Å, contoured at 4.5σ, is shown in red. (**D**) View of the ion-binding sites of the EcClC E148Q mutant. Atoms are represented as in (B).

The functional coupling between Cl^- ion conduction and gating in certain ClC channels (*5, 8, 9*) is compatible with the gating mechanism proposed in Fig. 5. The glutamate carboxyl group could be viewed as a Cl^- analog that displaces a conducting ion to interrupt flow. In this view, energetic interactions between the gate and Cl^- ions are easy to understand. Both internal and external Cl^- ion concentrations affect gating (*8, 9*). Further work will be required to understand the molecular details of coupling, but the structure offers many clues.

We describe in ClC channels a very simple form of gating in which local motions of an amino acid side chain lead to occlusion of the ion pathway. Compare the simplicity of this process to activation gating in K^+ channels, which involves global motions of transmembrane α helices (*1*). What are the advantages and disadvantages to gating by local versus global conformational changes? It seems to us that global changes create the opportunity to regulate gating. For example, large helical motions can be coupled to distant conformational changes elsewhere in the protein, allowing extramembranous domains to govern pore opening in response to ligand binding (*17–19*). In contrast, local conformational changes are probably only governable by local physical-chemical influences, such as changes in pH or ion composition. The effect of pH on the glutamate gate is consistent with the proposed role of ClC channels in bacterial acid resistance (*20*), and possibly the role of ClC channels in intracellular vesicle acidification (*7*). Further work is needed to understand the role of the glutamate gate in different ClC channels and why a subset of ClC channels from kidney naturally have substitution of the gate (*21*).

The open structure of the pore has fascinating implications for conduction principles in ion-selective channels. Despite their fundamentally different architectures, the ion pathways of K^+ and Cl^- channels are beginning to look more alike from a chemical point of view. In both cases, α-helix end charges (C-terminal for K^+ and N-terminal for Cl^-) are used to stabilize ions within the membrane (*2, 10, 22*), main-chain atoms (oxygen for K^+ and nitrogen for Cl^-) form selective ion-binding sites (*2, 4, 10*), and multiple ions are found very close together in a queue (*3*), presumably so that mutual destabilization will foster rapid conduction.

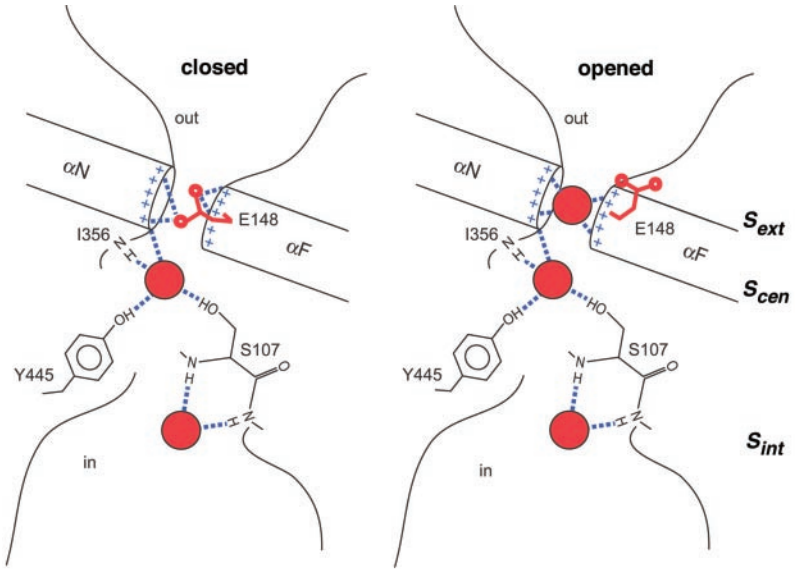

Fig. 5. Schematic drawing of the closed and opened conformation of a ClC chloride channel. In the closed conformation, the ion-binding sites S_{int} and S_{cen} are occupied by chloride ions, and the ion-binding site S_{ext} is occupied by the side chain of Glu^{148}. In the opened conformation, the side chain of Glu^{148} has moved out of binding site S_{ext} into the extracellular vestibule. S_{ext} is occupied by a third chloride ion. Chloride ions are shown as red spheres, the Glu^{148} side chain is colored red, and hydrogen bonds are drawn as dashed lines.

References and Notes

1. Y. Jiang *et al*., *Nature* **417**, 523 (2002).
2. D. A. Doyle *et al*., *Science* **280**, 69 (1998).
3. J. H. Morais-Cabral, Y. Zhou, R. MacKinnon, *Nature* **414**, 37 (2001).
4. Y. Zhou, J. H. Morais-Cabral, A. Kaufman, R. MacKinnon, *Nature* **414**, 43 (2001).
5. E. A. Richard, C. Miller, *Science* **247**, 1208 (1990).
6. M. Maduke, C. Miller, J. A. Mindell, *Annu. Rev. Biophys. Biomol. Struct.* **29**, 411 (2000).
7. T. J. Jentsch, V. Stein, F. Weinreich, A. A. Zdebik, *Physiol. Rev.* **82**, 503 (2002).
8. M. Pusch, U. Ludewig, A. Rehfeldt, T. J. Jentsch, *Nature* **373**, 527 (1995).
9. T. Y. Chen, C. Miller, *J. Gen. Physiol.* **108**, 237 (1996).
10. R. Dutzler, E. B. Campbell, M. Cadene, B. T. Chait, R. MacKinnon, *Nature* **415**, 287 (2002).
11. Monoclonal antibody [mouse immunoglobulin G (IgG)] against *S. typhimurium* ClC (StClC) was obtained as described (*23*). Total messenger RNA was isolated from the mouse hybridoma cells using TRIZOL reagents (Gibco BRL). The DNA encoding the variable region of the antibody was obtained by reverse transcription polymerase chain reaction (RT-PCR) by the 5′ RACE system (Gibco BRL). The antibody was sequenced using the RT-PCR product as template. *E. coli* ClC was purified in the detergent decylmaltoside (DM) as described (*10*). Mouse IgG was purified from mouse hybridoma cell culture supernatant using ion exchange chromatography (Q-sepharose, Pharmacia). Fab fragments were obtained by papain proteolysis followed by Q-sepharose chromatography. *E. coli* ClC and Fab were mixed in an OD_{280} ratio of 1:2.3. The complex was purified on a Superdex 200 column (Pharmacia) equilibrated in 150 mM NaCl, 10 mM tris-HCl (pH 7.5), and 10 mM DM. For crystallization, the NaCl concentration was lowered to 90 mM by dilution. For preparation of crystals in NaBr, the protein was dialyzed against a solution containing 90 mM NaBr. Crystals of the *E. coli* ClC Fab complex were grown in sitting drops at 20°C by equilibrating a 1:1 mixture of protein and reservoir solutions against the reservoir. The reservoir contained 28 to 31% polyethylene glycol (PEG 300), 50 mM glycine (pH 9.5), and 100 mM NaCl. For crystals grown in Br^-, NaCl was replaced by NaBr. Crystals were frozen in a stream of boiled-off nitrogen. The PEG 300 concentration was raised to 35% by dialysis before freezing. All data sets were collected on frozen crystals.
12. Point mutations were introduced by the QuikChange method (Stratagene) and confirmed by sequencing of the entire DNA insert. Capped RNA was transcribed from wild-type and mutated ClC-0 and injected into *Xenopus* oocytes. After 1 day, currents were measured by a two-electrode voltage clamp (OC-725B, Warner Instrument Corp.). Electrodes had a resistance of ~0.5 megohms (3 M KCl). The bath solutions contained 5 mM Hepes (pH 7.5), 2 mM $MgCl_2$, and 100 mM NaCl. For experiments at pH 5.0, Hepes was replaced with 5 mM citrate.
13. C. Miller, *Philos. Trans. R. Soc. London Ser. B* **299**, 401 (1982).
14. T. J. Jentsch, K. Steinmeyer, G. Schwarz, *Nature* **348**, 510 (1990).
15. M. F. Chen, T. Y. Chen, *J. Gen. Physiol.* **118**, 23 (2001).
16. C. Miller, M. M. White, *Ann. N.Y. Acad. Sci.* **341**, 534 (1980).
17. Y. Sun *et al*., *Nature* **417**, 245 (2002).
18. N. Unwin, A. Miyazawa, J. Li, Y. Fujiyoshi, *J. Mol. Biol.* **319**, 1165 (2002).
19. Y. Jiang *et al*., *Nature* **417**, 515 (2002).
20. R. Iyer, T. M. Iverson, A. Accardi, C. Miller, *Nature* **419**, 715 (2002).
21. S. Uchida *et al*., *J. Biol. Chem.* **268**, 3821 (1993).
22. B. Roux, R. MacKinnon, *Science* **285**, 100 (1999).
23. E. Harlow *et al*., *Antibodies: A Laboratory Manual* (Cold Spring Harbor Laboratory Press, Cold Spring Harbor, NY, 1989).
24. Z. Otwinowski, W. Minor, *Methods Enzymol.* **276**, 307 (1997).
25. J. Navaza, *Acta Crystallogr.* **A50**, 157 (1994).
26. K. Cowtan, *Joint CCP4 ESF-EACBM Newsl. Protein Crystallogr.* **31**, 34 (1994).
27. T. A. Jones, J. Y. Zou, S. W. Cowan, M. Kjeldgaard, *Acta Crystallogr.* **A47**, 110 (1991).
28. A. T. Brünger *et al*., *Acta Crystallogr.* **D54**, 905 (1998).

29. We thank T. Jensch for DNA encoding the ClC-0 channel, the staff at the National Synchrotron Light Source (NSLS) X25, the staff at Cornell High Energy Synchrotron Source (CHESS) A1, M. Zhou and O. Yifrach for assistance with electrophysiology, Y. Zhou for assistance in data collection, members of the MacKinnon laboratory for help at all stages of the project, and T. Y. Chen for manuscript critique. Supported by grants from NIH (R.M.). R.M. is an investigator of the Howard Hughes Medical Institute. Coordinates have been deposited into the Protein Data Bank under codes 10TS, 10TT, and 10TU.

23 January 2003; accepted 11 March 2003
Published online 20 March 2003;
10.1126/science.1082708
Include this information when citing this paper.

REPORTS

Ultrahigh-Density Nanowire Lattices and Circuits

Nicholas A. Melosh,[1,2] Akram Boukai,[1,2] Frederic Diana,[3] Brian Gerardot,[3] Antonio Badolato,[3] Pierre M. Petroff,[3] James R. Heath[1,2]*

We describe a general method for producing ultrahigh-density arrays of aligned metal and semiconductor nanowires and nanowire circuits. The technique is based on translating thin film growth thickness control into planar wire arrays. Nanowires were fabricated with diameters and pitches (center-to-center distances) as small as 8 nanometers and 16 nanometers, respectively. The nanowires have high aspect ratios (up to 10^6), and the process can be carried out multiple times to produce simple circuits of crossed nanowires with a nanowire junction density in excess of 10^{11} per square centimeter. The nanowires can also be used in nanomechanical devices; a high-frequency nanomechanical resonator is demonstrated.

One of the great challenges in developing nanofabrication patterning techniques involves the reduction of feature size, and the corresponding increase in pattern density, of various metal and semiconductor structures. Such device scaling has often been demonstrated as the most productive route toward developing more efficient and faster electronics circuitry. In addition, there is also the hope of eventually developing patterning techniques that begin to approach the feature sizes and densities that are characteristic of macromolecules. Such approaches would open up new opportunities for constructing devices and circuits that can interface with, for example, biological systems. To this end, a tremendous amount of effort has been put into reducing the feature sizes of the traditional, parallel patterning techniques of photolithography, as well as more specialized, serial patterning approaches such as electron beam lithography (EBL). All of these approaches face fundamental challenges, but for one-of-a-kind devices, EBL is the highest resolution technique available (*1*).

Standard metrics for the resolution of a patterning process are the line width and center-to-center distance (pitch) of an array of aligned nanowires. EBL has yielded patterns with nanowire diameters as small as 20 nm (*1*). However, the pitch is limited to ~60 nm because of "noise" in the processing steps required to translate a pattern that has been written into resist material into an actual array of aligned, conducting wires. For example, a thin layer of metal is typically evaporated onto the resist layer, adhering directly to the substrate in the windows patterned through the resist layer. The resist is then dissolved in the appropriate solvent, causing the newly unsupported metal film to tear free, or "lift off," leaving only the metal that was in direct contact with the substrate. However, for very small features, the metal-substrate adhesion area is quite small, and those features may also lift off. This problem is reversed at very small pitches, because the cohesion of the metal film may prevent or disrupt the lift-off process.

[1]California Nanosystems Institute, University of California, Box 956905, Los Angeles, CA 90095, USA. [2]California Institute of Technology, Pasadena, CA 91125, USA. [3]California Nanosystems Institute, University of California, Santa Barbara, CA 93106, USA.

*To whom correspondence should be addressed. E-mail: heath@caltech.edu